Diyala Journal of Engineering Sciences

Journal homepage: https://djes.info/index.php/djes

ISSN: 1999-8716 (Print); 2616-6909 (Online)

Effect of Hump Configurations of Porous Square Cavity on Free Convection Heat Transfer

Ahmed A. Fadhil[1], Itimad D.J. Azzawi[1*], I.M. Mahbubul[2] and M. Hasannuzaman[3]

[1]Department of Mechanical Engineering, University of Diyala, 32001 Diyala, Iraq
[2]Institute of Energy Engineering, Dhaka University of Engineering & Technology, Gazipur 1707, Bangladesh
[3]Higher Institution Centre of Excellence (HICoE), UM Power Energy Dedicated Advanced Centre (UMPEDAC), Level 4, Wisma R&D, University Malaya, Jalan Pantai Baharu, 59990 Kuala Lumpur, Malaysia

ARTICLE INFO

Article history:
Received January 1, 2023
Revised June 7, 2023
Accepted June 17, 2023
Available online September 1, 2023

Keywords:
Wavy porous square enclosure
Hump configuration
Number of humps
Free convection
Heat transfer enhancement.

ABSTRACT

Free convection is widely used in engineering applications, including solar energy, electronic devices, nuclear energy and heat exchangers. A computational simulation utilising Ansys Fluent-CFD was used to examine the natural convection heat transfer inside a square cavity filled with pure water and saturated metal foam as a porous medium (porosity ε=0.9). The enclosure's lower wavy wall exhibits a high temperature (T_h), whereas the side and upper walls display a low temperature (T_c). For different Rayleigh numbers, the study examines hump configuration and the bottom wall hump number (N). The predominant design of heat transmission was improved using the circular hump design parameters of ε=0.9, N=4 and T_c=25 °C for different Ra. The novelty of the research included determining the optimal design for the square enclosure. This approach involved estimating the effects of hump configuration and the number of humps for the bottom wall of the enclosure. These parameters have not been studied yet. The optimum case showed the highest heat transfer coefficient (*h*) at the circular hump, *N*=4 and Ra=30×10^3, whereas the standard case obtained *N*=0 and Ra=5×10^3. The CFD simulation results indicate that the primary objective of the study was achieved through the optimal design, resulting in a significant enhancement of hydrothermal performance for heat transfer enhancement and energy enhancement 1.13 times compared with the standard case.

1. Introduction

Owing to the substantial and persistent growth in energy consumption rates and the rising scarcity of conventional energy sources accompanied by high prices, a result of industrial development following the mid-20th-century industrial revolution, the energy crisis is considered one of the most critical problems confronting the world. Thus, researchers are deliberately attempting to improve the performance of heat exchange systems and change their size to reduce their rates of thermal energy usage. In subsequent studies, several researchers focused on free convection inside cavities and fluid flow without magnetohydrodynamics (MHD) because of its wide applications. The researchers focused on several techniques that proved to be very effective in improving heat transfer. One of these techniques is manipulation and changes in the geometry of the cavities. Other techniques include nanofluid usage, porous medium and magneto-hydrodynamic (MHD).

A numerical simulation was conducted to study the natural convection in a triangle

* Corresponding author.
E-mail address: itimaddawood_eng@uodiyala.edu.iq
DOI: 10.24237/djes.2023.160301

enclosure filled with water and a porous medium for various Rayleigh numbers (Ra), heater locations (P_h), heater lengths (L_h) and inclination angles (θ). An increase in heat transfer indices with higher values of (L_h) and (θ=0) was observed at high levels of Ra. Response surface methodology (RSM) was applied for optimisation investigation of aspect ratios (L/H) (Ra) and porosity, and the highest heat transfer was recorded at the lowest value of porosity and the highest L/H value [1]. Numerous studies on the utilisation of nanofluids in containers of varying shapes, with and without the impact of magnetic field intensity, have been conducted. These studies revealed an improvement in heat transfer through an elevation in its indicators with an increase in Ra and nanoparticle concentration, while also considering alterations in container dimensions. These results were obtained from multiple sources [2–5]. Al-Damook et al. evaluated the natural convection with MHD and metal foam in an L-shaped cavity. The study found that MHD and oblique angles of a cavity have a widespread impact on heat transfer. As porosity decreases, heat transfer indicators improve, along with reduced surface temperature and entropy generation and an increase in aspect ratio. These findings are relevant to the field of academic research on heat transfer [6]. Previous literature on heat transfer has been extensively reviewed by numerous authors, who have investigated porosity and its potential to enhance heat transfer in porous fluids. The findings indicate that porosity has a significant impact on heat transfer, and researchers are recommended to explore its utilisation in future research endeavours [7-8]. Several researchers previously investigated the impact of magnetic fields on heat transfer in liquid-filled cavities with varying geometries. They observed that higher Hartman numbers (Ha) corresponded to greater electrical conductivity and vortex motion within the cavities, ultimately resulting in improved heat transfer rates. They also studied the MHD direction, which significantly increase and enhance heat transfer [9–15]. Azizul et al. studied numerically free convection inside a square cavity filled with nanofluid and having an inner solid block. When the straight bottom wall of the cavity was replaced with a wavy wall, significant enhancement in free convection heat transfer was achieved [16]. Khalil et al. used computational simulation (CFD-Fluent) to study natural convection heat transfer inside a wavy porous trapezoidal enclosure. According to a study, an increase in heat transfer of 3.37 times was achieved by utilising a combination of four waves (N=4) and an amplitude of 20 mm (a=20 mm); further enhancement was observed at a Hartman number of 40 (Ha=40) [17]. A previous study was conducted to analyse free convection inside a square enclosure with oblique undulation-sided walls. Numerical simulation findings reveal that increasing the amplitude of the two-sided undulation walls of the cavity slightly enhanced the transfer of heat [18]. Several studies on the utilisation of square-geometry structures to enhance heat transfer have been conducted. The results demonstrate that the implementation of this approach effectively enhances the heat transfer effect, as evidenced by previous research [19-20]. The influence of the aspect ratio of the right-side wall of a square enclosure on natural convection was studied with various numbers of waves by numerical simulation, The simulation findings showed that the cooling efficiency of the heat source increased gradually with growth increasing in aspect ratio [21]. The increase in aspect ratio and Ra leads to the increase in heat transmission inside a horizontal and shallow wavy chamber that has a bottom wavy wall and upper and side straight walls; heat transfer declined with an increase in the non-dimensional length of wave according to simulation findings [22]. The placement of the geometry affects the heat transfer enhancement given that the acceleration, in this case, influences the movement of the liquid inside the enclosure, as well as increases the movement of the liquid and its mixing due to the difference in liquid temperature. Moolya et al. investigated free convection within a rectangular enclosure filled with the fluid and showed a significant enhancement in local Nusselt number as an indicator of heat transfer due to an inclination of the geometry of the rectangular cavity [23]. The

work focuses on the enhancement of the free convection inside a porous wavy square chamber filled with pure water and saturated porous media with porosity level of (ε=0.9). The analysis also considers the impact of hump configuration for the bottom wall of the container and the number of humps (N) on heat transfer rates. Recent literature on wavy porous square cavities has not fully analysed these parameters. The computational simulation of ANSYS FLUENT-CFD-R20 for laminar flow, 2D steady state and single phase utilised in this investigation to explain the effect of hump configure and *N* on heat transfer indicators, namely, heat transfer coefficient (*h*) and heat transfer rate (*Q*).

2. Numerical methodology

2.1 Model description and problem characterisation

The current study focuses on addressing heat transfer inside porous square cavity issues through the examination of some parameters to improve their thermal performance, ultimately resulting in enhanced heat transfer indicators. The model used in this study is a 2D square cavity (H×H) containing pure water and a saturated metal foam porous medium shown in Figure 1. The cavity's side and top walls have a low temperature of T_c=25 °C. The bottom wall has a variable hot temperature (T_h) expressed in terms of Ra, with investigations into the hump configuration (circular, triangle, square, up semi-circle, and down semi-circle) and number of humps (N=0, 1, 2, 3 and 4) with no-slip conditions (v=u=0).

2.2 Mesh study

The mesh verification study selected a suitable grid size to guarantee that the algorithms used in this analysis are unaffected by grid size or size elements. This approach would minimise the computer load, amount of time and expense required to complete the investigation. Therefore, a porous square wavy cavity surface with the following grid size value (2, 1.75, 1.5, 1.25, 1, 0.8, 0.7 and 0.5) was divided into eight structures (triangles mesh). Heat transfer coefficient (*h*) and heat transfer rate (*Q*) at Ra=(5 and 30)×10^3 observation values were utilised to assess this verification. The results showed no changes in (*h* and *Q*) at the size element of 0.7 mm and below. Hence, all computational approaches in this work should depend on this information to produce precise results.

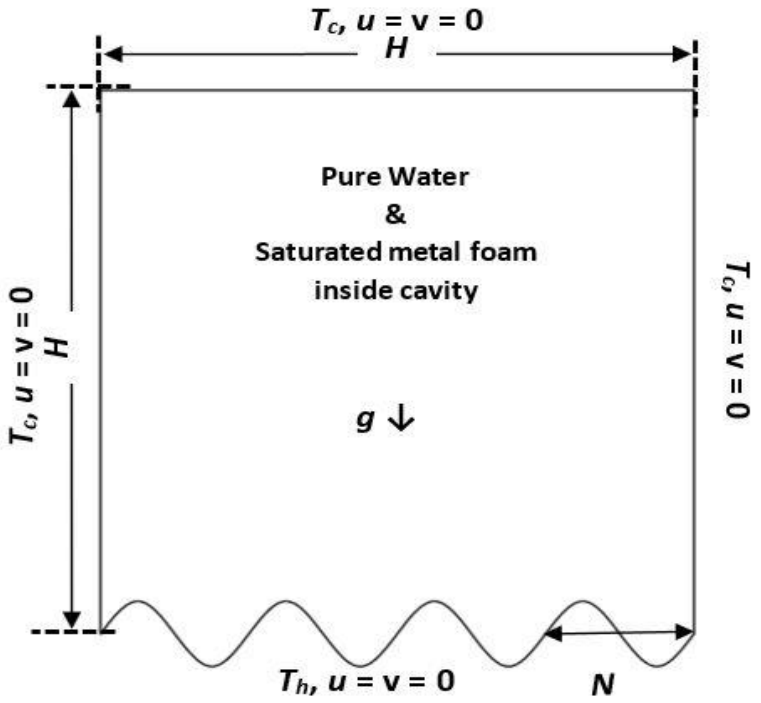

Figure 1. Model used with boundary conditions.

2.3 Mathematical formula and the hypotheses

The Ansys-Fluent program was used to analyse the natural free convection heat transmission rate and thermal efficiency within a square enclosure containing pure water and saturated metal foam as a porous material. The simulations were performed with specific parameters, including 2D, laminar, steady state, incompressible flow, single-phase and water fluid properties. The hydraulic properties of water, except for density, remain unaffected by temperature increases, thereby validating the use of the Forchheimer–Darcy law in this simulation. In addition, given the significant inertial effects observed, the governing equations [1] used are as follows:

Continuity equation

$$\frac{\partial \mathrm{u}}{\partial \mathrm{x}}+\frac{\partial \mathrm{v}}{\partial \mathrm{y}}=0 \quad (1)$$

x-momentum equation

$$\rho\left(\mathrm{u}\frac{\partial \mathrm{u}}{\partial \mathrm{x}}+\ v\frac{\partial v}{\partial \mathrm{y}}\right)=\ -\varepsilon^{2}\frac{\partial \mathrm{p}}{\partial \mathrm{x}}+\ \varepsilon\mu\left(\frac{\partial^{2}u}{\partial \mathrm{x}^{2}}+\frac{\partial^{2}u}{\partial y^{2}}\right)-\frac{\rho \mathrm{C}\varepsilon^{2}}{K^{0.5}}u|\mathrm{U}|-\frac{\mu\varepsilon^{2}}{K}u \quad (2)$$

y-momentum equation

$$\rho\left(\mathrm{u}\frac{\partial \mathrm{u}}{\partial \mathrm{x}}+\ v\frac{\partial v}{\partial \mathrm{y}}\right)=\ -\varepsilon^{2}\frac{\partial \mathrm{p}}{\partial \mathrm{y}}+\ \varepsilon\mu\left(\frac{\partial^{2}v}{\partial \mathrm{x}^{2}}+\frac{\partial^{2}v}{\partial y^{2}}\right)+\varepsilon^{2}\rho\beta\mathrm{g}(\mathrm{T}-\mathrm{Tc})-\frac{\rho \mathrm{C}\varepsilon^{2}}{K^{0.5}}u|\mathrm{U}|-\frac{\mu\varepsilon^{2}}{K}u \quad (3)$$

energy equation

$$u\frac{\partial \mathrm{T}}{\partial \mathrm{x}}+v\frac{\partial \mathrm{T}}{\partial \mathrm{y}}=\alpha_{e}\left(\frac{\partial^{2}\mathrm{T}}{\partial \mathrm{x}^{2}}+\frac{\partial^{2}\mathrm{T}}{\partial \mathrm{y}^{2}}\right) \quad (4)$$

where $|U|=\sqrt{u^{2}+v^{2}}$, α_e=$\frac{k_e}{\rho C_p}$ or $\alpha_e=\frac{\varepsilon k_w+(1-\epsilon)k_{Al}}{\rho C_p}$ is the effective thermal diffusivity, and k_e is the effective thermal conductivity [17].

The ratio of the enhanced heat transfer coefficient (h_{Enhanced}) to the standard heat transfer coefficient ($h_{standard}$) is referred to as heat transfer enhancement and can be represented by the following formula:

$$\left(\frac{h_{Enhanced}}{h_{standard}}\right), \quad (5)$$

where ($h_{standard}$) is the standard heat transfer coefficient for a straight square chamber (*N*=0).

The ratio of the enhanced thermal energy transfer rate ($Q_{Enhanced}$) to the standard thermal energy transfer rate ($Q_{standard}$) referred to as the energy enhancement and can be represented by the following formula:

$$\left(\frac{Q_{Enhanced}}{Q_{standard}}\right). \quad (6)$$

where ($Q_{standard}$) is standard energy enhancement for a straight square chamber (N=0).

2.4 Procedure of computational solution

Upon inputting the designated parameters, specifically the activation of energy and imposition of laminar flow, the Ansys-Fluent was configured with the setup field. Moreover, input water flow characteristics (Density ρ=997 kg/m^3, Specific heat cp=4180 J/kg.K, Thermal conductivity k=0.607 W/m.K, Dynamic viscosity μ=0.000891 Ns/m^2 and Thermal Expansion Coefficient β=0.000247 1/K) [17] activated cell zone condition (porous zone with the magnitude of porosity) and added boundary condition and reference value. Coupled algorithm is the second-order upwind scheme for pressure, momentum and energy in each X–Y direction. The equations are then iteratively solved in several attempts to achieve convergence in the results after hybrid initialisation and run calculation. Subsequently, the indices of the heat transfer rate are calculated in a porous square enclosure. The residual values of the monitors are established to be below 10^{-6} for the continuity, momentum and energy.

3. Results and discussion

3.1 Validation study

A study was conducted to assess the current ANSYS Fluent-CFD-R20 code and compare it with the work of Calcagni et al. [24] on square cavities at Ra=10^4. The resulting contour graphics for isotherm lines at heat source length=1/5 (left) and at heat source length=4/5 (right) were found to be highly similar, as illustrated in Figures 2 (A and B). Furthermore, numerical calculations were conducted for all cases of Ra=10^3, 10^4, 10^5 and 10^6 for the above heat sources, based on the experimental findings of Calcagni et al. [24]. A considerable level of convergence was observed when comparing the findings with the prior research, with an error rate that did not exceed 3% to 4%, as shown in Figure 2 (C).

3.2 Effect of hump configuration

A numerical simulation was performed to examine the effect of the lower wall hump configuration of the porous square enclosure. Figure 5 presents the graphic contours of isotherms and stream functions that show the effect of hump configuration on heat transfer indicators (*h* and *Q*) inside the enclosure for various Ra and ε=0.9, T_c=25 °C.

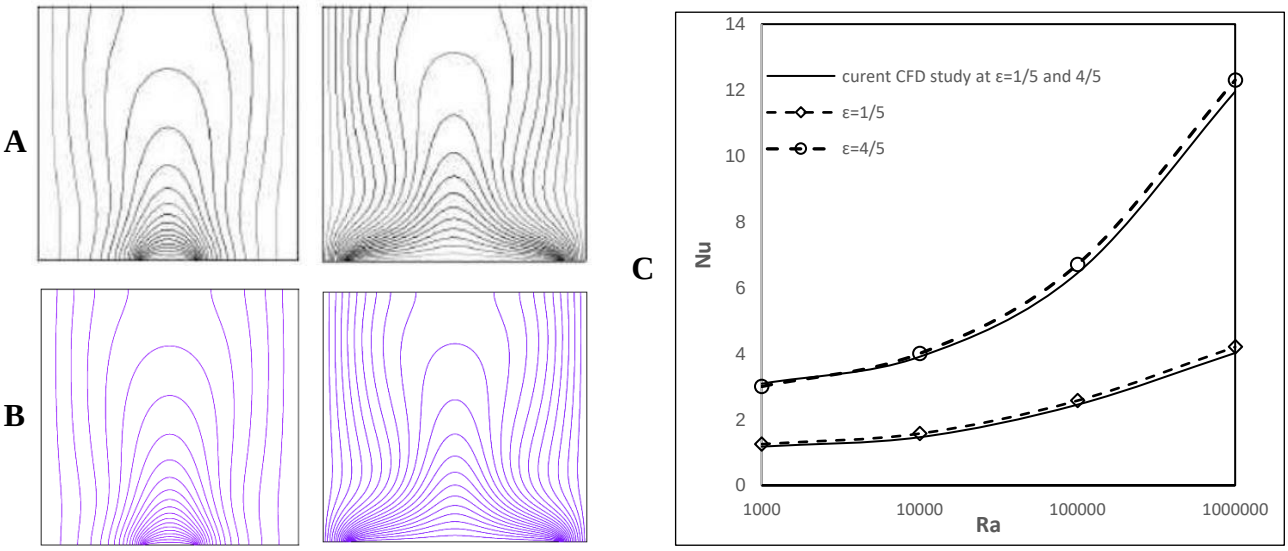

Figure 2. Validation isotherm lines at heat source length=1/5 (Left) and isotherms at heat source length=4/5 (Right) of Calcagni et al. [24] (A), current CFD study (B) and Calcagni et al. [24] with data (C).

Figure 3 (left) illustrates that the values of *h* remain nearly constant for the first three values of Ra= $(5,10,15)\times10^3$ for all hump configurations except square. Thereafter, *h* gradually increases with increasing Ra. The circular hump at Ra=30×10^3 resulted in the highest (h) value. The heat transfer rate inside the enclosure increased linearly with increasing Ra values, as depicted in Figure 3 (right), leading to improved heat transfer. The comparison of humps showed that the square hump was the least effective in enhancing heat transfer. Furthermore, consistency in the magnitudes of *h* and *Q* was observed for the straight wall (standard) and triangle hump, indicating convergence. By contrast, the circular hump achieves high heat transfer rate values at the maximum value of Ra (Ra=30×10^3). Furthermore, Figure 4 provides numerical estimations for the influence of hump configuration on heat transfer enhancement and energy enhancement as functions of Ra compared with a straight wall (standard). The figure also illustrates the augmentation of heat transfer and energy through different hump configurations, excluding the square hump. The values of heat transfer enhancement and energy enhancement are almost constant at all Ra levels. A marginal decrease was observed at a high value of Ra (Ra=30×10^3), indicating that the circular hump achieved more significant heat transfer convection and thermal energy enhancement. The findings from Eqs. (5) and (6) indicate that a square hump resulted in the poorest heat transfer and thermal energy when compared with a flat or straight bottom wall. Figure 5 (right) shows isotherm graphic contours for various hump configurations. The temperature gradient within the enclosure increases as the hump configuration changes,

leading to an increase in Ra. As a result, heat transfers from a hot, wavy bottom wall to the cold sides and upper walls. The circular hump and Ra=30×10^3 are found to be the most favourable conditions for achieving optimal heat transfer, whereas the square hump results in the worst outcomes. These observations can be attributed to greater thermal interference occurring at higher Ra values, owing to increased flow intensity. This effect is reversed at lower Ra values. Figure 5 (left) illustrates the formation of two large-scale vortices within an enclosure, rotating in the opposite direction while maintaining comparable dimensions and strengths, as characterised by the same Ra and hump number (N). However, the flow strength is enhanced from (Ψ_{max}=0.001603) at the flat bottom wall to (Ψ_{max}=0.001616) at the circular hump bottom wall at Ra=5×10^3. Similarly, the maximum flow strength also improves from (Ψ_{max}=0.01354) at the flat bottom wall to (Ψ_{max}=0.01617) at the circular hump and Ra=30×10^3. The presence of a circular hump within an enclosure results in the movement of vortices from the hot lower space to the cold upper space. In the case of a square hump, a stream function is hindered by pressure drops and collisions between vortices within the hump. Consequently, circulation in the upper space of the enclosure is impeded.

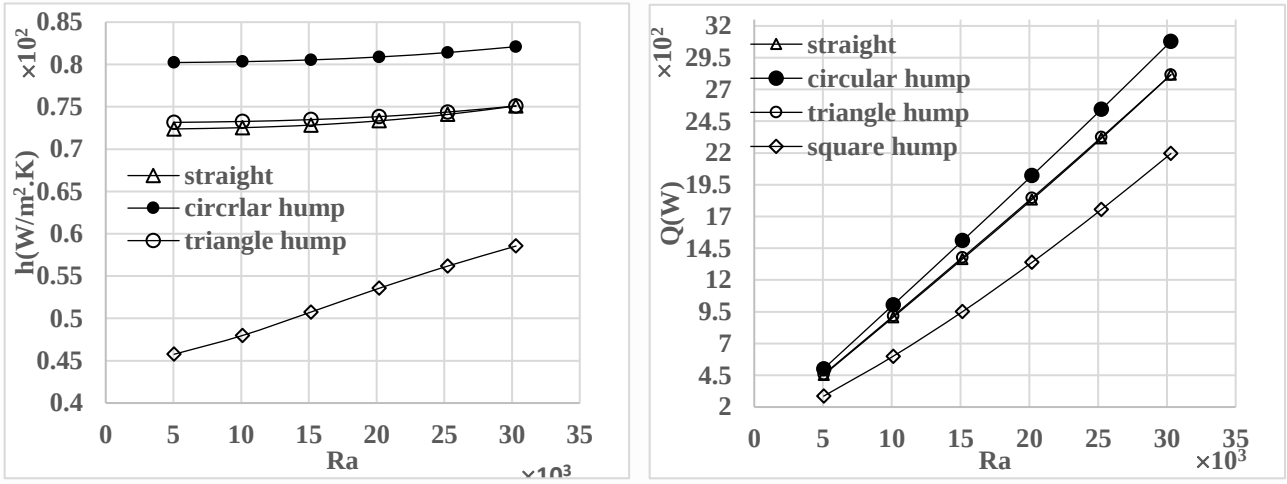

Figure 3. Heat transfer coefficient *h* (Left) and heat transfer rate *Q* (Right) for different Ra and hump configure at *N*=4, T_c=25 °C, ε=0.9.

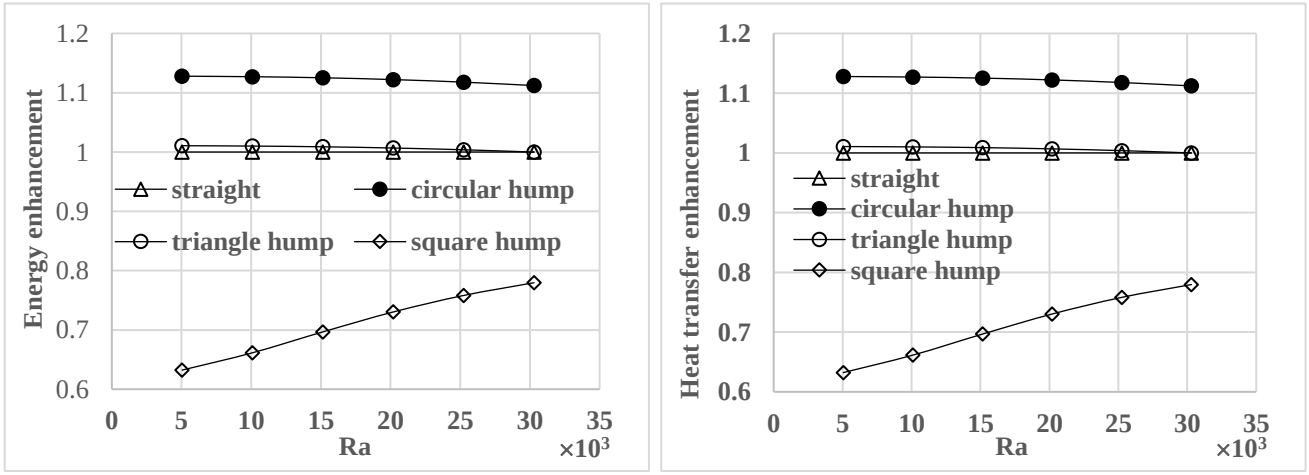

Figure 4. Energy enhancement (Left) and heat transfer enhancement (Right) for various Ra and hump configure at N=4, T_c=25 °C and ε=0.9.

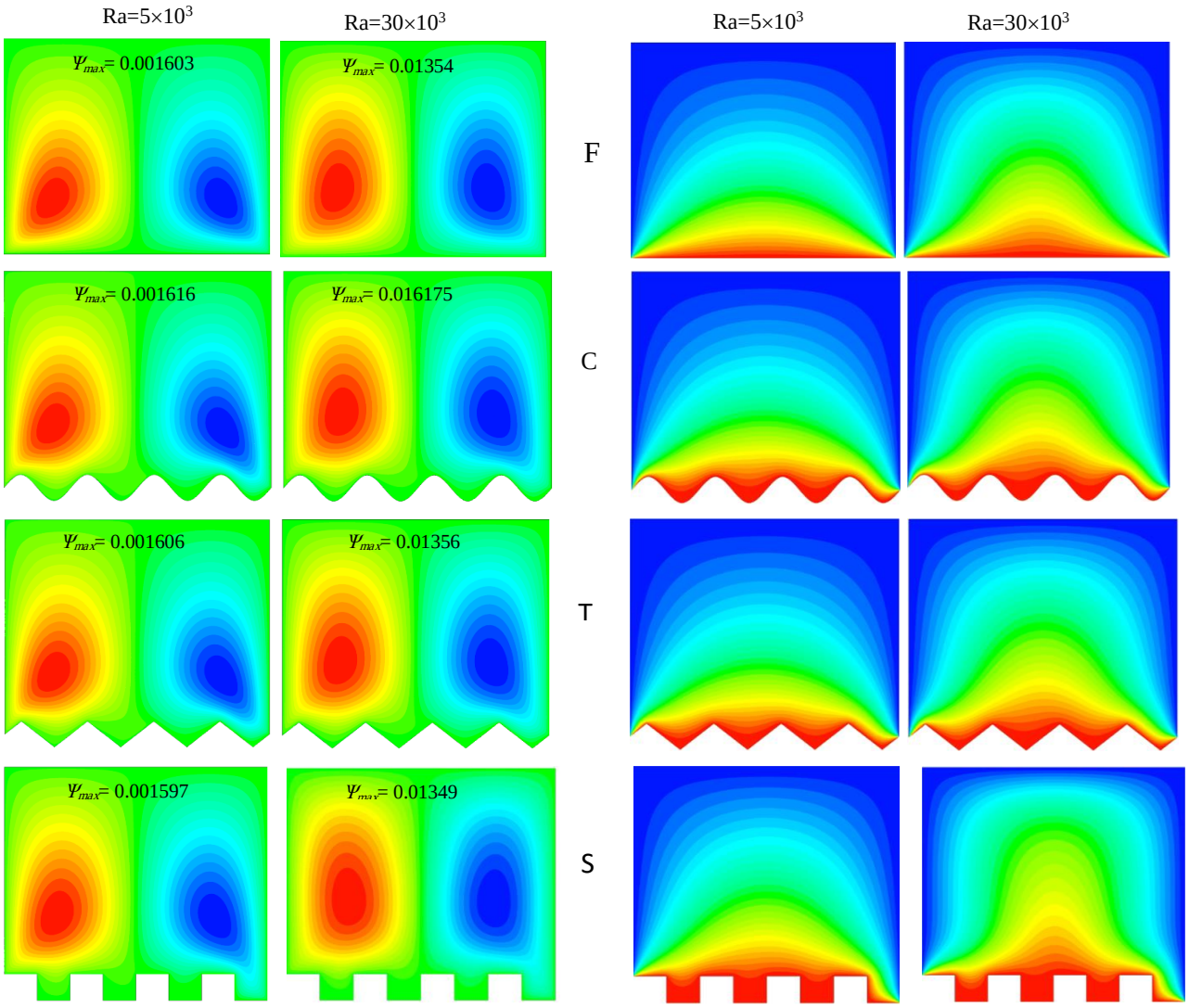

Figure 5. Stream functions (Left) and isotherms (Right) at Ra=(5 and 30)×10^3 for different configuration of hump flat bottom wall (*F*), circular hump (*C*), triangle hump (*T*) and square hump (*S*) at T_c=25 °C, *N*=4, ε=0.9.

After identifying and selecting the optimal case from the illustrated cases in Figure 5, namely, the circular hump, numerical simulations were conducted to evaluate whether any enhancements in heat transfer and thermal energy can be observed by comparing the upward and downward semi-circular configurations. The simulation findings indicate that the circular hump configuration remains the optimal scenario as it generates the most elevated values for heat transfer indices, *h* and *Q*. Figure 6 (left) illustrates that the circular hump arrangement attained the greatest value of *h*, which remained constant for the three initial Ra=(5, 10, 15) ×10^3 prior to progressively escalating with increasing Ra. The highest value of *h* was observed at the circular hump and Ra=30×10^3. The heat transfer rate, as measured by parameter *Q*, exhibits a nearly linear increase with increasing Ra. Figure 6 (Right) illustrates that the highest heat transfer rate is observed at the circular hump with a Ra of 30×10^3. Figure 7 displays streamline and isotherm contours for circular, upstream semi-circular and downstream semi-circular humps. Figure 7 (right) depicts a thermal gradient from the hot lower wall to the cold side and top walls of the cavity, as well as a decrease in heat transmission

in the upstream semi-circular and downstream semi-circular hump configurations when compared with the circular hump. Figure 7 (left) shows how the flow strength decreased from (Ψ_{max}=0.001616) at the circular hump to (Ψ_{max}=0.001581) at the downstream semi-circular hump at Ra=5×10^3 and from (Ψ_{max}=0.016175) to (Ψ_{max}=0.0134) at Ra=30×10^3 due to low flow and the low influence of vortices movement. Figure 7 displays a pressure drop that arises in conjunction with the downstream semi-circular hump configuration. The effect of the circular hump on heat transfer is detailed in the above section.

3.3 Effect of bottom wall's hump number (N)

The impact of *N* on heat transfer and thermal energy was investigated using numerical simulation on a hot bottom wall. Figure 10 shows streamlines (left) and isotherms (right) of graphic contours for Ra=5×10^3 as the minimum Ra and Ra=30×10^3 as the maximum, with the following boundary conditions: T_c=25 °C, ε=0.9 and circular hump. In the present study, we examined several hump numbers (*N*=0, 1, 2, 3 and 4). The simulation results indicate that an increase in N and Ra leads to a stronger flow and higher temperature intensity. The stream functions exhibit the highest strength (Ψ_{max}= 0.016175) at a high Ra (Ra=30×10^3) when *N*=4, resulting in the expansion of vortex movement towards the upper space of the enclosure, counter to the flow along the straight bottom wall (*N*=0). Figure 10 (right) depicts heat transfer from a hot lower wall to a cold, upper and side walls. The increase in the value of the parameter *N* leads to the dominance of heat transfer by convection, counter to the case, where *N*=0, presenting dominant conduction. At *N*=4 and Ra=30×10^3, a higher amount of heat is

.

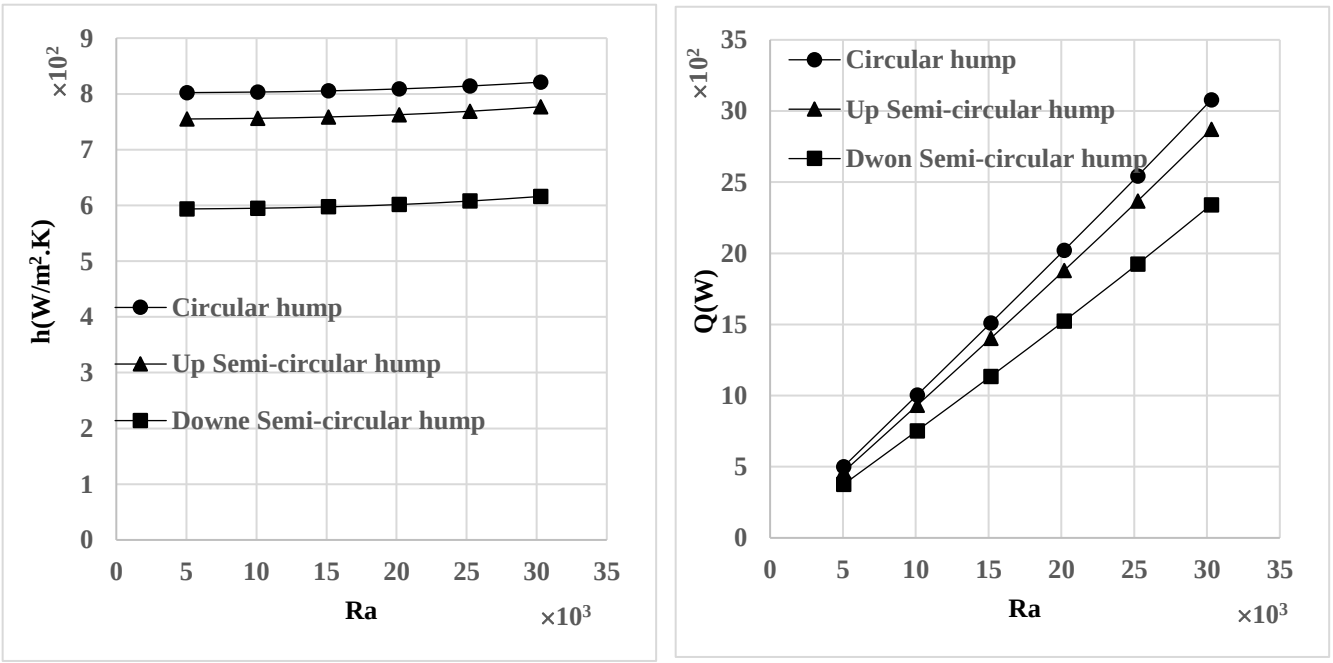

Figure 6. Heat transfer coefficient *h* (Left) and heat transfer rate *Q* (Right) for different Ra and hump configuration at *N*=4, T_c=25 °C and ε=0.9.

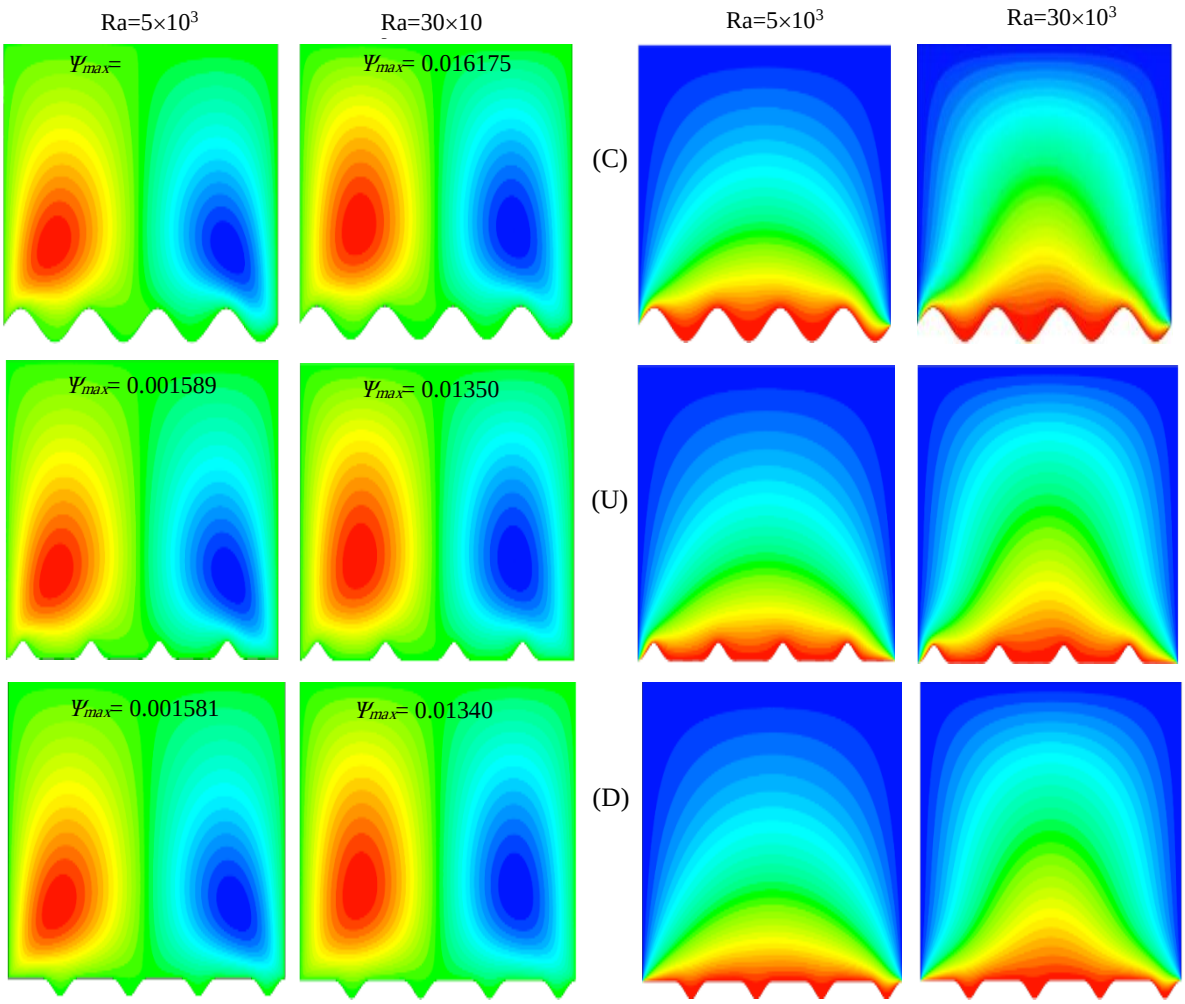

Figure 7. Stream functions (Left) and Isotherms (Right) at Ra=(5 and 30) × 10^3 for various hump configure circular hump (*C*), Up semi-circular hump (*U*) and Down semi-circular hump (*D*) at N=4, Tc= 5 °C and ε=0.9.

transferred in a porous square enclosure due to the presence of significant thermal advection. This phenomenon occurs at the maximum value of Ra, which corresponds to the maximum intensity of flow contrast between regions with different Ra values. Figure 8 shows the effect of the number of humps on the heat transfer coefficient and heat transfer rate. The study shows enhancements in heat transfer and thermal energy within a square cavity that contains pores, where the Ra varies. The *h* values remain constant for the three initial values of Ra, namely, (5, 10, 15) ×10^3. However, at Ra=30×10^3, the *h* value peaks. This increase in convection within the cavity is directly related to an increase in *N* and Ra, resulting in improved heat transfer. The value of *h* was found to be the lowest when additional straight walls (*N*=0) were used, whereas the highest value of *h* was observed when continuity increased with *N*, as shown in Figure 8 (left). Figure 8 (right) demonstrates that as the Ra and *N* increases, the values of *Q* inside the enclosure steadily increases in behaviour that resembles linearity. The highest rate of heat transfer was achieved at Ra=30×10^3. The lowest value of *Q* occurred at Ra=5×10^3 and *N*=0. The highest value of *Q* was observed when *N*=4, indicating that *N*=4 achieved optimal enhanced heat transfer. The emergence of upward vortices could facilitate the intermingling of fluid layers. Figure 9 illustrates the impact of the number of

humps (*N*) on heat transfer and thermal energy enhancement. At a constant Ra, heat transfer enhancement and energy enhancement experience *N* increases. Moreover, this enhancement is found to gradually lessen with increasing Ra. The similarity between the behaviour of *N*=0 and *N*=1 is observed with the enhancement from 1 at *N*=0 to 1.07 at *N*=1, whereas the heat transfer and thermal energy remain constant for all Ra. The highest heat transfer enhancement and energy enhancement occurred at *N*=4 and Ra=5×10^3, representing 1.13 times the standard case at boundary conditions: T_c=25 °C, ε=0.9 and circular hump. This finding indicates that *N*=4 is the optimal parameter.

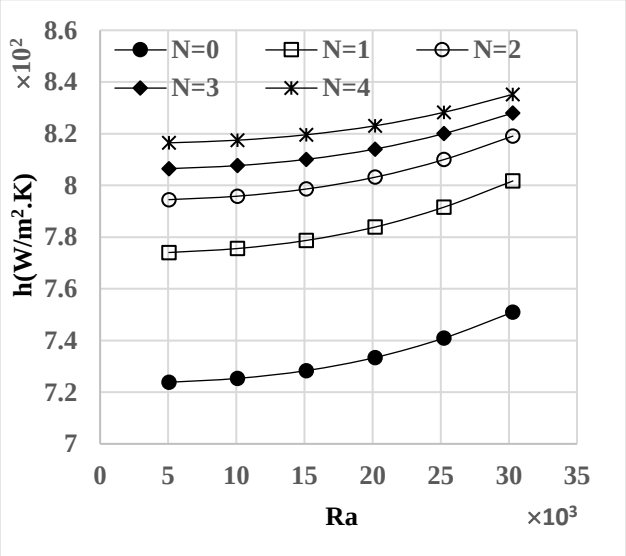

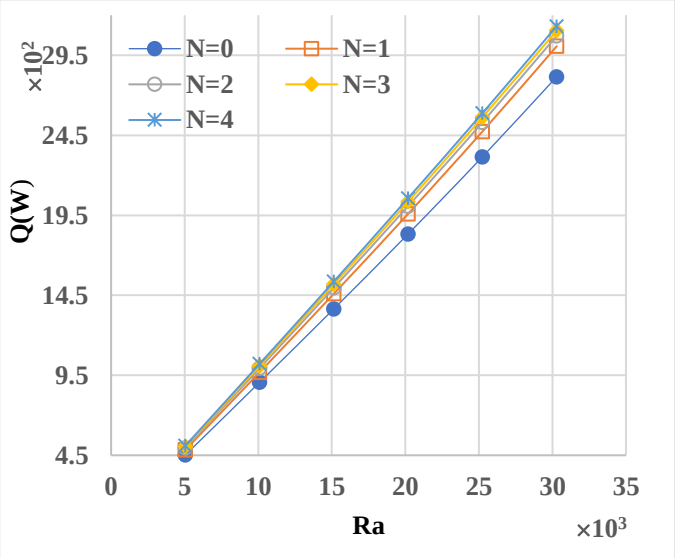

Figure 8. Heat transfer coefficient *h* (Left) and heat transfer rate *Q* (Right) for different Ra and *N* at Tc=25 °C, ε=0.9, and circular hump.

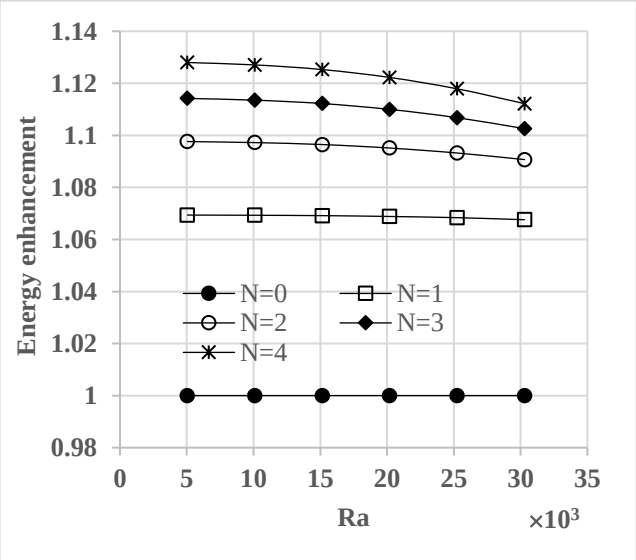

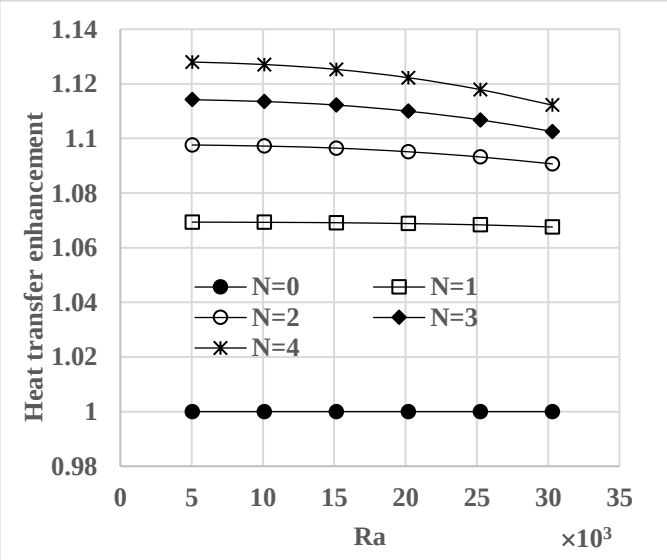

Figure 9. Energy enhancement (Left) and heat transfer enhancement (Right) for different Ra and *N* at Tc=25 °C, ε=0.9 and circular hump.

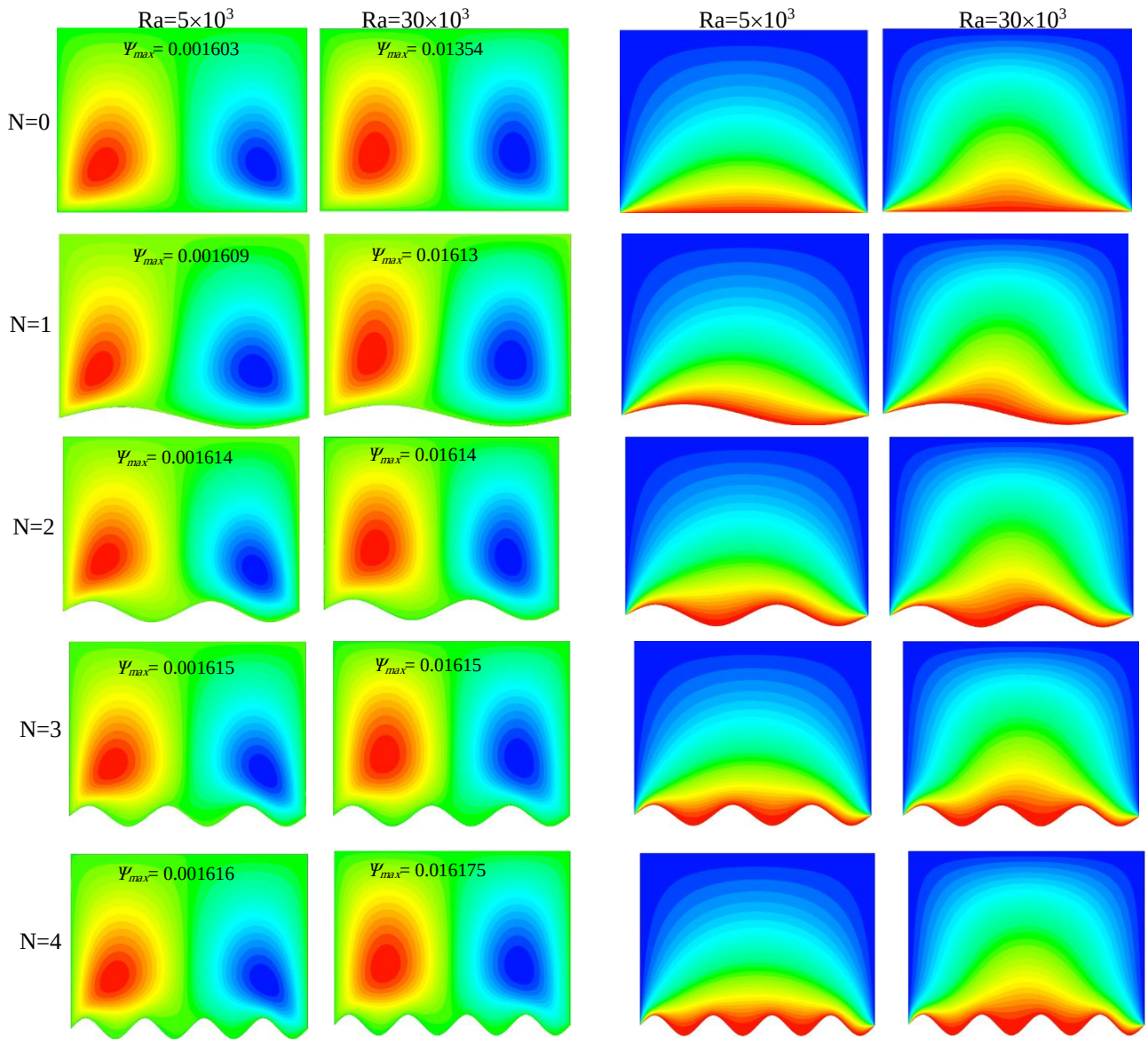

Figure 10. Stream functions (Left) and Isotherms (Right) at Ra=(5 and 30)× 10^3 for different *N* at ε=0.9, T_c=25 °C, and circular hump.

4. Conclusions

The current study has investigated the impacts of a hump configuration and *N* on free convection heat transfer in a porous square chamber containing pure water and saturated by a porous medium (ε=0.9). The influence of different hump configurations (circular, triangle, square, up semi-circular and down semi-circular) and numbers of the lower wall humps (*N*=0, 1, 2, 3 and 4) are examined with a range of Ra (5, 10, 15, 20, 25 and 30) ×10^3. Ansys Fluent-CFD was applied in this analysis to observe the enhancement of heat transfer indicators (*h* and *Q)*.

The main conclusions are outlined, as follows:

1. The utilisation of a hump configuration instead of a straight bottom wall results in improvements in the heat transfer coefficient (h), heat transfer rate (Q), heat transfer enhancement and thermal energy enhancement. For various Ra, the average improvement in *h* and *Q* at the circular hump is 1.13 times greater than that of the standard case (*N*=0).
2. Circular hump achieves the highest values of *h* and *Q* when considering the effect of up semi-circular and down semi-circular hump.

A comparison amongst circular, up semi-circular and down semi-circular humps is conducted to show their influences on free convection inside the square cavity.

3. Figure 8 demonstrates that the heat transfer indicators exhibit improvement with an increase in the number of lower wall humps (*N*). The highest average enhancement of heat transfer indices for *h* and *Q*, compared with the standard case (*N*=0), is 1.13 times at *N*=4 across various Ra.

Subsequently, this experiment proved that the wavy bottom wall enclosure with a circular hump provides an enhancement in heat transfer and thermal energy more than the straight bottom wall enclosure, and it supported the hypotheses mentioned in a large number of previous literatures.

References

[1] I. D. J. Azzawi and A. Al-damook, "Multi-objective optimum design of porous triangular chamber using RSM," *International Communications in Heat and Mass Transfer*, vol. 130, Jan. 2022, doi: 10.1016/j.icheatmasstransfer.2021.105774.

[2] R. Mohebbi, M. Izadi, H. Sajjadi, A. A. Delouei, and M. A. Sheremet, "Examining of nanofluid natural convection heat transfer in a Γ-shaped enclosure including a rectangular hot obstacle using the lattice Boltzmann method," *Physica A: Statistical Mechanics and its Applications*, vol. 526, Jul. 2019, doi: 10.1016/j.physa.2019.04.067.

[3] M. Shekaramiz, S. Fathi, H. A. Ataabadi, H. Kazemi-Varnamkhasti, and D. Toghraie, "MHD nanofluid free convection inside the wavy triangular cavity considering periodic temperature boundary condition and velocity slip mechanisms," *International Journal of Thermal Sciences*, vol. 170, Dec. 2021, doi: 10.1016/j.ijthermalsci.2021.107179.

[4] B. AL-Muhjaa and K. Al-Farhany, "Numerical Investigation of the Effect of Baffle Inclination Angle on Nanofluid Natural Convection Heat Transfer in A Square Enclosure," *Al-Qadisiyah Journal for Engineering Sciences*, vol. 12, no. 2, pp. 61–71, Jun. 2019, doi: 10.30772/qjes.v12i2.589.

[5] S. Aghakhani, A. H. Pordanjani, M. Afrand, M. Sharifpur, and J. P. Meyer, "Natural convective heat transfer and entropy generation of alumina/water nanofluid in a tilted enclosure with an elliptic constant temperature: Applying magnetic field and radiation effects," *Int J Mech Sci*, vol. 174, May 2020, doi: 10.1016/j.ijmecsci.2020.105470.

[6] A. Al-damook and I. D. J. Azzawi, "MHD Natural Convection of Water in An L-Shaped Container Filled with An Aluminium Metal Foam," *J Heat Transfer*, Feb. 2022, doi: 10.1115/1.4055942.

[7] A. Kasaeian *et al.*, "Nanofluid flow and heat transfer in porous media: A review of the latest developments," *International Journal of Heat and Mass Transfer*, vol. 107. Elsevier Ltd, pp. 778–791, Apr. 01, 2017. doi: 10.1016/j.ijheatmasstransfer.2016.11.074.

[8] C. C. Cho, "Effects of porous medium and wavy surface on heat transfer and entropy generation of Cu-water nanofluid natural convection in square cavity containing partially-heated surface," *International Communications in Heat and Mass Transfer*, vol. 119, Dec. 2020, doi: 10.1016/j.icheatmasstransfer.2020.104925.

[9] Y. Ma, R. Mohebbi, M. M. Rashidi, O. Manca, and Z. Yang, "Numerical investigation of MHD effects on nanofluid heat transfer in a baffled U-shaped enclosure using lattice Boltzmann method," *J Therm Anal Calorim*, vol. 135, no. 6, pp. 3197–3213, Mar. 2019, doi: 10.1007/s10973-018-7518-y.

[10] C. C. Liao and W. K. Li, "Assessment of the magnetic field influence on heat transfer transition of natural convection within a square cavity," *Case Studies in Thermal Engineering*, vol. 28, Dec. 2021, doi: 10.1016/j.csite.2021.101638.

[11] B. Chandra Shekar, C. Haritha, and N. Kishan, "Magnetohydrodynamic convection in a porous square cavity filled by a nanofluid with viscous dissipation effects," *Proceedings of the Institution of Mechanical Engineers, Part E: Journal of Process Mechanical Engineering*, vol. 233, no. 3, pp. 474–488, Jun. 2019, doi: 10.1177/0954408918765314.

[12] S. Sivasankaran and C. J. Ho, "Effect of temperature dependent properties on MHD convection of water near its density maximum in a square cavity," *International Journal of Thermal Sciences*, vol. 47, no. 9, pp. 1184–1194, Sep. 2008, doi: 10.1016/j.ijthermalsci.2007.10.001.

[13] B. Ghasemi, S. M. Aminossadati, and A. Raisi, "Magnetic field effect on natural convection in a nanofluid-filled square enclosure," *International Journal of Thermal Sciences*, vol. 50, no. 9, pp. 1748–1756, Sep. 2011, doi: 10.1016/j.ijthermalsci.2011.04.010.

[14] P. X. Yu, J. X. Qiu, Q. Qin, and Z. F. Tian, "Numerical investigation of natural convection in a rectangular cavity under different directions of uniform magnetic field," *Int J Heat Mass Transf*, vol. 67, pp. 1131–1144, 2013, doi: 10.1016/j.ijheatmasstransfer.2013.08.087.

[15] M. Sathiyamoorthy and A. Chamkha, "Effect of magnetic field on natural convection flow in a liquid gallium filled square cavity for linearly

heated side wall(s)," *International Journal of Thermal Sciences*, vol. 49, no. 9, pp. 1856–1865, Sep. 2010, doi: 10.1016/j.ijthermalsci.2010.04.014.

[16] F. M. Azizul, A. I. Alsabery, and I. Hashim, "Heatlines visualisation of mixed convection flow in a wavy heated cavity filled with nanofluids and having an inner solid block," *Int J Mech Sci*, vol. 175, Jun. 2020, doi: 10.1016/j.ijmecsci.2020.105529.

[17] W. H. Khalil, I. D. J. Azzawi, and A. Al-damook, "The optimisation of MHD free convection inside porous trapezoidal cavity with the wavy bottom wall using response surface method," *International Communications in Heat and Mass Transfer*, vol. 134, May 2022, doi: 10.1016/j.icheatmasstransfer.2022.106035.

[18] W. Al-Kouz, K. B. Saleem, and A. Chamkha, "Numerical investigation of rarefied gaseous flows in an oblique wavy sided walls square cavity," *International Communications in Heat and Mass Transfer*, vol. 116, Jul. 2020, doi: 10.1016/j.icheatmasstransfer.2020.104719.

[19] D. K. Mandal, N. Biswas, N. K. Manna, R. S. R. Gorla, and A. J. Chamkha, "Magneto-hydrothermal performance of hybrid nanofluid flow through a non-Darcian porous complex wavy enclosure," *European Physical Journal: Special Topics*, vol. 231, no. 13–14, pp. 2695–2712, Sep. 2022, doi: 10.1140/epjs/s11734-022-00595-6.

[20] P. S. Rao and P. Barman, "Natural convection in a wavy porous cavity subjected to a partial heat source," *International Communications in Heat and Mass Transfer*, vol. 120, Jan. 2021, doi: 10.1016/j.icheatmasstransfer.2020.105007.

[21] P. Barman and P. S. Rao, "Effect of aspect ratio on natural convection in a wavy porous cavity submitted to a partial heat source," *International Communications in Heat and Mass Transfer*, vol. 126, Jul. 2021, doi: 10.1016/j.icheatmasstransfer.2021.105453.

[22] Y. Varol and H. F. Oztop, "Free convection in a shallow wavy enclosure," *International Communications in Heat and Mass Transfer*, vol. 33, no. 6, pp. 764–771, Jul. 2006, doi: 10.1016/j.icheatmasstransfer.2006.02.004.

[23] S. Moolya and S. Anbalgan, "Optimization of the effect of Prandtl number, inclination angle, magnetic field, and Richardson number on double-diffusive mixed convection flow in a rectangular domain," *International Communications in Heat and Mass Transfer*, vol. 126, Jul. 2021, doi: 10.1016/j.icheatmasstransfer.2021.105358.

[24] B. Calcagni, F. Marsili, and M. Paroncini, "Natural convective heat transfer in square enclosures heated from below," in *Applied Thermal Engineering*, Nov. 2005, pp. 2522–2531. doi: 10.1016/j.applthermaleng.2004.11.032.